B04-report

14.4-keV Solar Axion Search: Preliminary Results with a TES Microcalorimeter and Iron-57 Absorber

Yuta Yagi (Ph.D. candidate)

The University of Tokyo[2],
Institute of Space and Astronautical Science / JAXA[1]

Collaborators

Tasuku Hayashi[3,4,7], Keita Tanaka[1,2], Rikuta Miyagawa[1,2], Ryo Ota[1,2], Noriko Y. Yamasaki[1,2,3], Kazuhisa Mitsuda[1,3,4], Rumi Sato[5], Nao Yoshida[5], Mikiko Saito[5], Takayuki Homma[5], Shohei Mori[6], Yoshiki Nishida[6], Naoko Iyomoto[6]

1. Japan Aerospace Exploration Agency
2. 東京大学 THE UNIVERSITY OF TOKYO
3. International Center for Quantum-field Measurement System for Studies of the Universe and Particles
4. 国立天文台 NAOJ National Astronomical Observatory of Japan
5. WASEDA University 早稲田大学
6. 九州大学 KYUSHU UNIVERSITY
7. 立教大学

What is the axion?

- A hypothetical elementary particle proposed to solve the strong CP problem (R.D. Peccei and H.R. Quinn 1977)
- One of cold dark-matter candidates in the universe
- Axion-photon conversion is allowed in electric or magnetic fields.
- Magnetic dipole transition in a nucleus (7Li, 57Fe, 83Kr, 169Tm, etc.) can emit axions

axion-photon coupling

Primakoff conversion

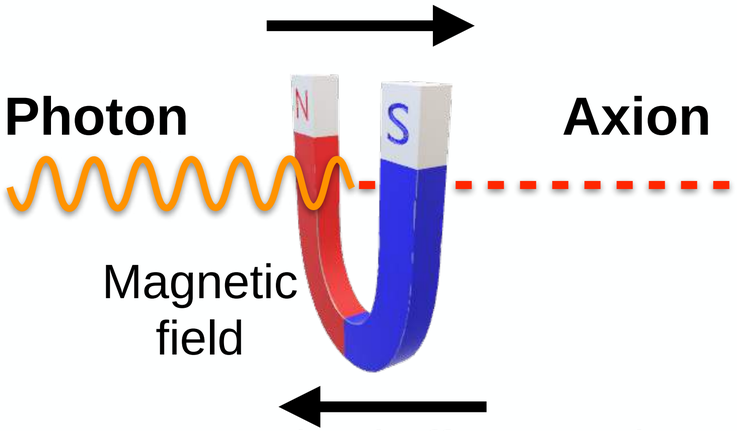

Inverse Primakoff conversion

axion-nucleon coupling

Magnetic dipole transition

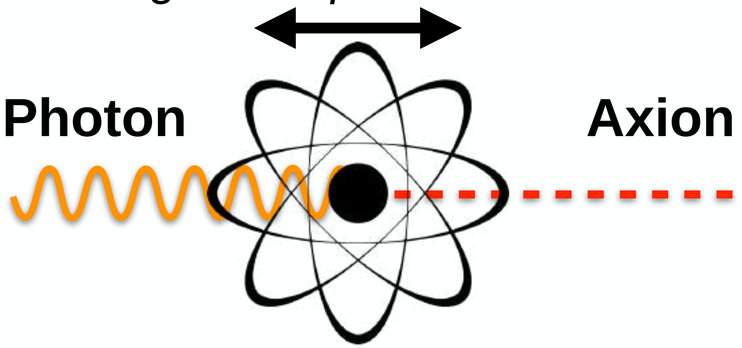

Expected solar axion spectrum

Sun

axion-photon coupling

Internal magnetic field

kT ~ 1.3 keV

Photon

Continuum spectrum

kT ~ 1.3 keV

Axion

Blackbody radiation

axion-nucleon coupling

Excitation

14.4 keV

Photon

Deexcitation

^{57}Fe in the solar core

Line spectrum

14.4 keV

Axion

Earth

14.4 keV

Photon

^{57}Fe of an absorber

Expected hadronic solar axion spectrum

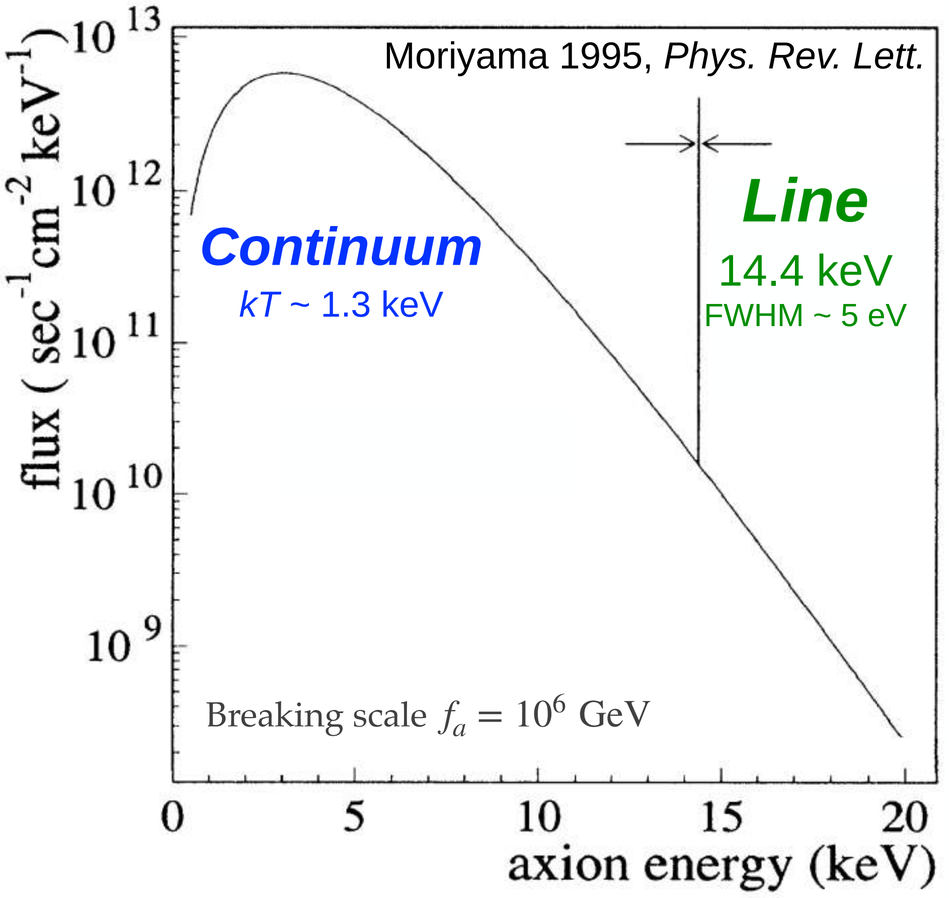

Focus on the intrinsic energy of 14.4-keV nuclear transition, which is independent of the axion mass

Advantages of solar axion search using 57Fe nuclei

- Reactions in the stellar core are independent of whether axions constitute the primary component of dark matter.
- Axions, with no theoretical mass limits, require exploration across a wide mass range. However, detection methods based on nuclear interactions allow for focus on the intrinsic energy levels of atomic nuclei, irrespective of axion mass.
- Line spectrum detection offers the advantage of conducting experiments on a relatively smaller scale compared to large-scale experiments requiring massive electromagnet for continuous spectrum detection.
- Abundance of ^{57}Fe nuclei in the sun, in contrast to other atoms with magnetic dipole transitions (^{7}Li, ^{83}Kr, ^{169}Tm, etc.), results in a significantly larger flux.
- Iron-57 exhibits axion-nucleon coupling in both solar radiation and terrestrial absorption, eliminating uncertainties associated with axion-photon coupling.

Expected hadronic solar axion spectrum

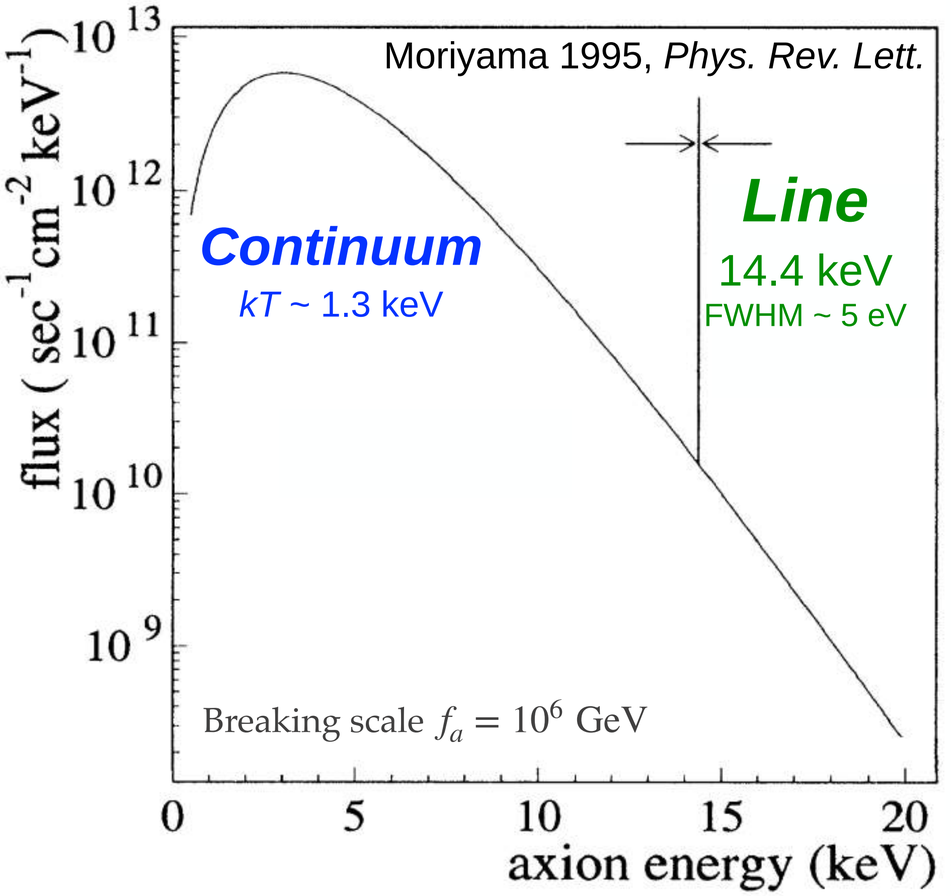

Previous studies using semiconductor Si detectors

Solar axion mass constraints using axion-nucleon coupling with iron-57

	Nucleon	Size	Mass	Time	Constraint
Namba 2007 **Si PIN photodiode**	^{57}Fe foil	35 um × 28 mm × 28 mm	197 mg	13.92 day	*ma* ≦ 216 eV (95% C.L.)
Derbin+ 2011 **Si(Li) detector**	57Fe	70 mm diameter, 30 mg/cm2	1.14 g	44.8 day	ma ≦ 145 eV (95% C.L.)
ISAI project **SOI detector**	^{57}Fe foil	40 um × 32 mm × 32 mm	~ 200–300 mg	→ *Tsuru-san's talk*	

Namba (2007) experimental system

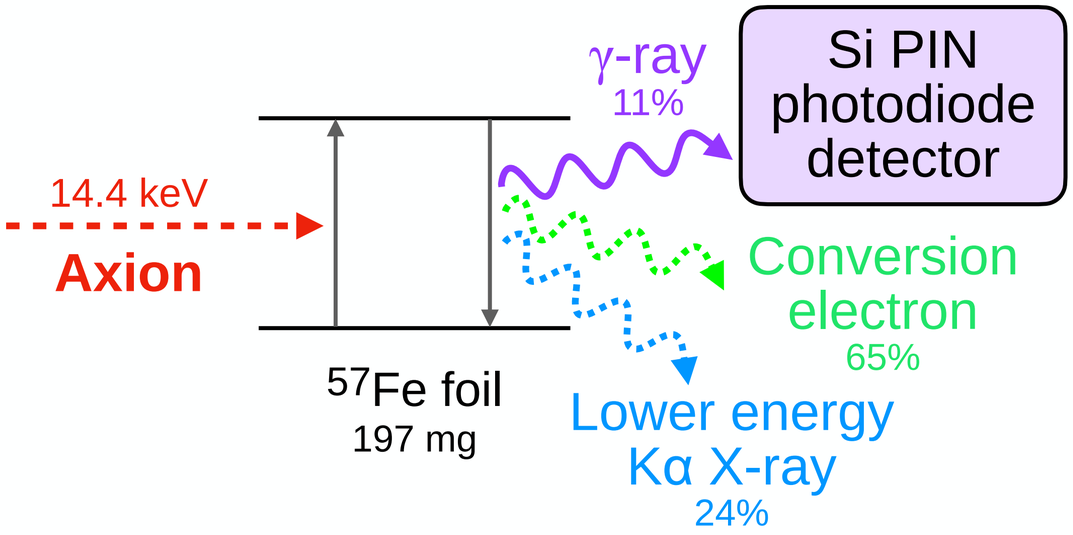

- Iron-57 branching ratio of 14.4-keV γ-rays — 10.5%
  That of conversion electrons and lower energy X-rays — 89.5%
- Detection efficiency of photodiode for 14.4 keV γ-ray — 14.8%
  (cf. Derbin+ 2011 Si(Li) detector — 8.91%)
  (cf. Onuki+ 2023 SOI detector, ISAI — 14.9%)
- **Total detection efficiency after deexcitation — 1.6%**
  (cf. Derbin+ 2011 Si(Li) detector — 0.94%)
  (cf. Onuki+ 2023 SOI detector, ISAI — 1.6%)

Detection efficiency is low
because only gamma rays can be detected

TES microcalorimeter for X-ray observation

Superconducting Transition Edge Sensor (TES) microcalorimeter

Sub-mm size “thermal detector with transition edge”

For X-ray observation

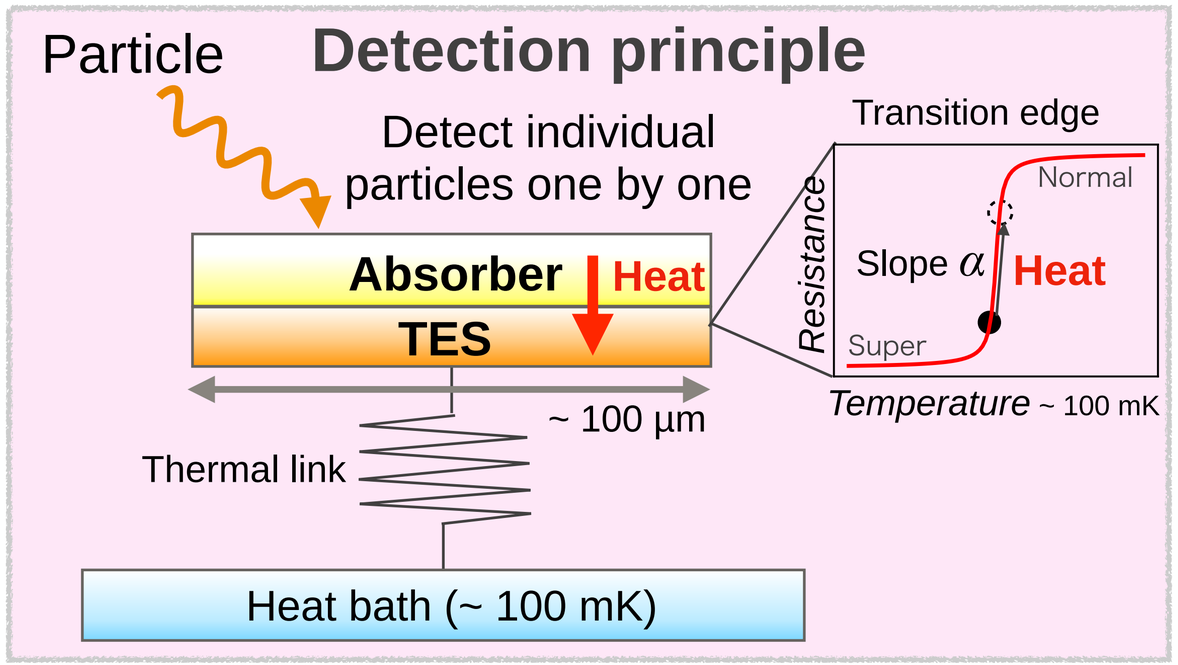

Energy resolution

$$\Delta E \propto \sqrt{\frac{CT^2}{\alpha}}$$

C: Heat capacity

T: Temperature

α: Slope ($= \ln R / \ln T$)

Single pixel

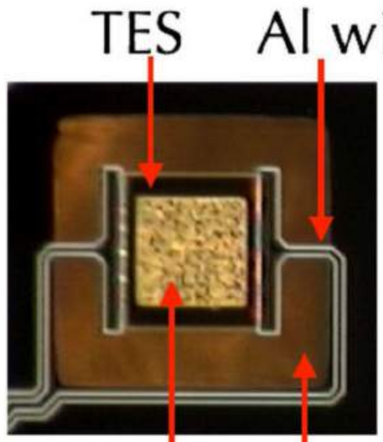

Muramatsu+ 2016, *J. Low Temp. Phys.*

Our group (1-pixel), Akamatsu+ 2009

$\Delta E = 2.79 \pm 0.29$ eV @ 5.9 keV

Our group (1-pixel), Muramatsu+ 2020

$\Delta E = 15.67^{+2.86}_{-2.66}$ eV @ 13.9 keV

64-pixel array

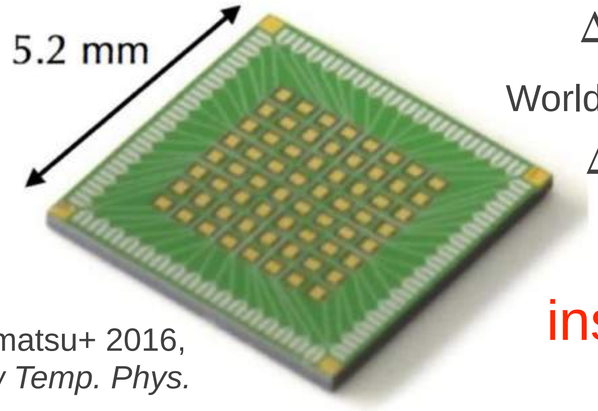

Muramatsu+ 2016, *J. Low Temp. Phys.*

Our group (64-pixel), Muramatsu+ 2016

$\Delta E = 7.84 \pm 0.57$ eV @ 5.9 keV

World record (208-pixel), Smith+ 2021

$\Delta E = 1.97 \pm 0.01$ eV @ 5.9 keV

→ Use ^{57}Fe absorber instead of X-ray absorber for solar axion

Advantages of using TES microcalorimeter

Semiconducting Si detector	Superconducting TES microcalorimeter
ΔE ~ 500 eV	ΔE ~ 2 eV (theoretically) Low noise at cryogenic temperature
Total detection efficiency ~ 1% Detects only gamma rays	Total detection efficiency ~ 70% Capable of self-absorbing gamma rays, conversion electrons, and low-energy X-rays in iron absorbers
Large mass of converted material due to the use of ^{57}Fe foil	1-pixel absorber 100-um square × tens of um = a few ug of ^{57}Fe → Arrayed to increase mass
Just build low background environment that can operate at room temperature	Need anti-coincidence detector that can operate at cryogenic temperature

Observation sensitivity of TES array

3σ upper limit of total detection rate per unit mass of iron-57 in the lab. (events/day/kg)

$$R = \frac{\sqrt{9 b_{\mathrm{pixel}} N t \eta \Delta E + (9/2)^2} + 9/2}{t M_{^{57}\mathrm{Fe,pixel}} N \alpha_{\mathrm{TES}}}$$

b_{pixel}: BDG rate (counts/s/pixel/keV)
N: the number of pixels
t: exposure time (s)
η: fudge factor
ΔE: energy resolution (eV)
$M_{^{57}\mathrm{Fe,pixel}}$: iron-57 mass per pixel (g/pixel)
α_{TES}: detection efficiency

(i) if $9 b_{\mathrm{pixel}} N t \eta \Delta E \ll (9/2)^2$ (Photon limit)

$$R = \frac{9}{t M_{^{57}\mathrm{Fe,pixel}} N \alpha_{\mathrm{TES}}}$$

(ii) if $9 b_{\mathrm{pixel}} N t \eta \Delta E \gg (9/2)^2$ (Background limit)

$$R = \frac{\sqrt{9 b_{\mathrm{pixel}} \eta \Delta E}}{M_{^{57}\mathrm{Fe,pixel}} \alpha_{\mathrm{TES}} \sqrt{tN}} \propto \frac{1}{\alpha^{1/4} M_{^{57}\mathrm{Fe,pixel}}^{3/4} \alpha_{\mathrm{TES}}} \sqrt{\frac{b_{\mathrm{pixel}} T}{tN}}$$

Observation sensitivity of TES array

All background limits

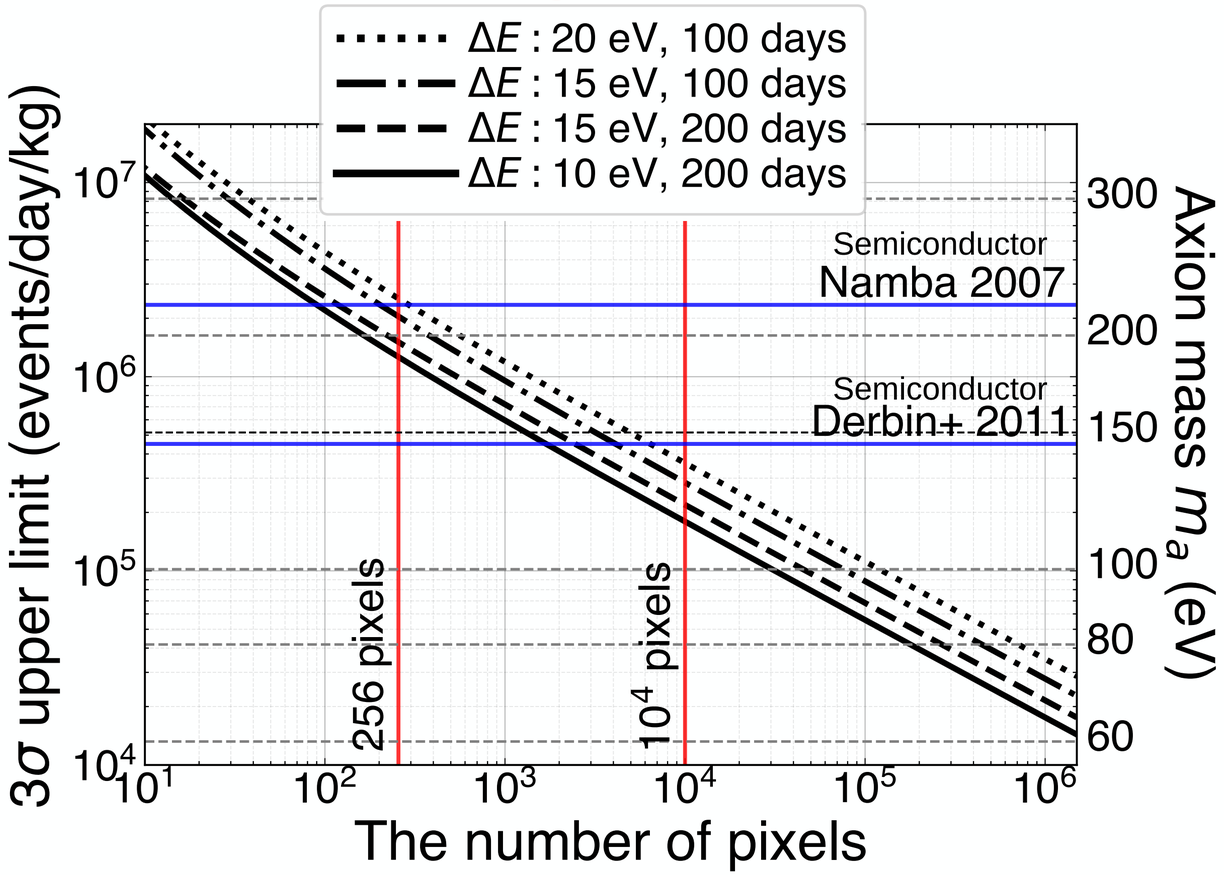

Yagi+ 2023, *J. Low Temp. Phys.*

Breaking scale $f_a = 10^6$ GeV

Absorber $= 100\ \mu\mathrm{m} \times 100\ \mu\mathrm{m} \times 10\ \mu\mathrm{m}$

BGD rate $= 1.0 \times 10^{-2}$ counts/s/cm^2/keV (with anti-coincidence detector)
$= 1.0 \times 10^{-6}$ counts/s/pixel/keV

Degradation of TES performance due to magnetic field

The spectroscopic performance of TES could degrade under a magnetic field made by ferromagnetic iron absorber

Magnetic simulation

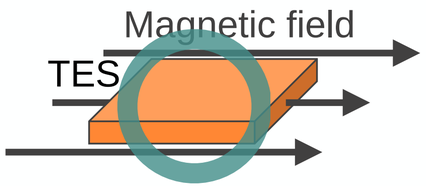

No change

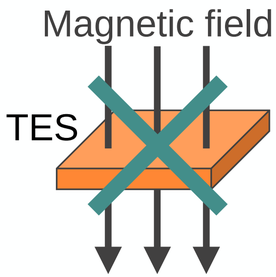

Make the sensitivity worse

Maehisa+ (LTD17 poster)

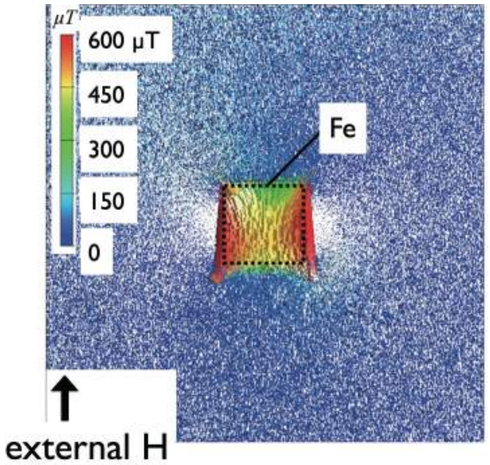

When the distance between TES and 5-μm thick Fe exceeds 30 μm, the vertical magnetic field is less than 1 μT.

Measured RT curve in the vicinity of Fe

TES-Fe distance: 60 μm
Fe thickness: 10 μm

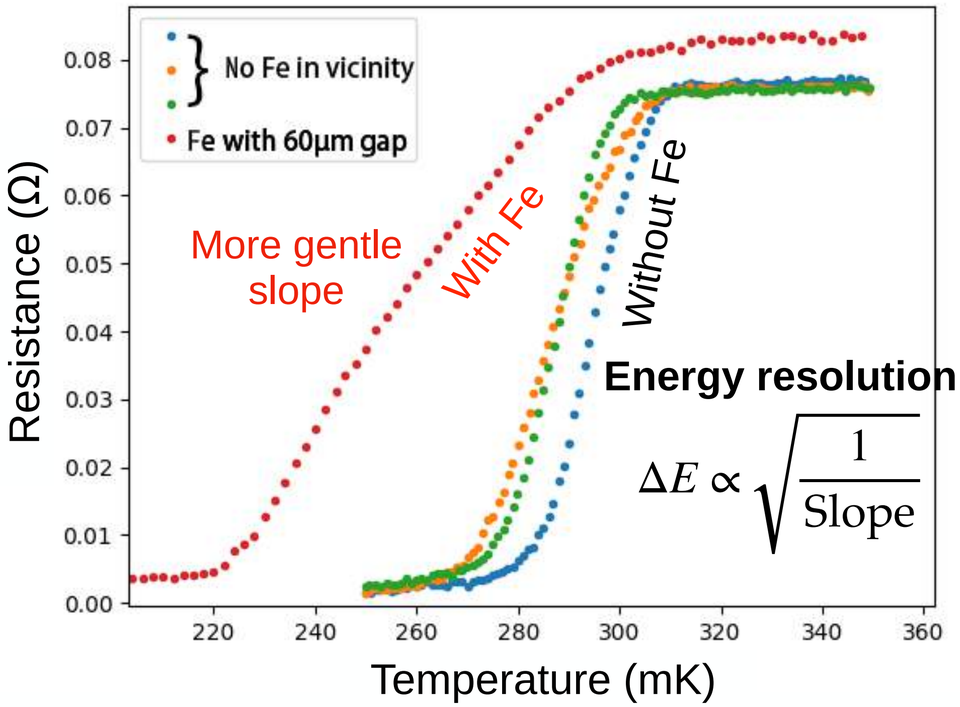

Konno+ 2020, *J. Low Temp. Phys.*

Structure to reduce the influence of iron magnetism

Placing Fe absorber at a distance laterally from TES
and thermally linking them with a highly conductive strap

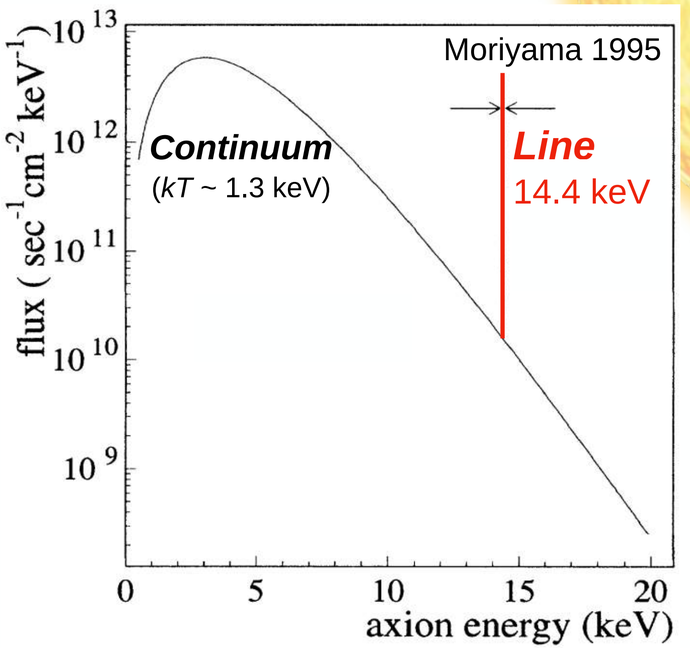

Need to fabricate a test device
and confirm the performance

Challenges in fabricating TES for axion

Issues/Challenges	Solutions/Improvements
Iron-57 used as absorber is expensive (~ 1M yen/gram), necessitating an efficient deposition method.	Opting for electroplating, a targeted chemical reaction method, instead of widespread techniques like evaporation or sputtering for cost-effective coating of specific areas.
Processing pure iron is uncommon, leading to an undeveloped deposition process. The coated area is small (100 μm square), making thickness control challenging.	As part of the development, collaboration with Waseda University, specializing in electroplating, for the deposition of the iron absorber.
Due to the increased thermal conduction distance from absorber, it is necessary to deposit films of materials with high thermal conductivity, such as Fe absorber and Au strap.	Successfully achieved Fe and Au electroplating with thermal conductivities, ≳ 1 W/m/K@4 K for Fe and > 3.5 W/m/K@200 mK for Au

Iron (III) oxide powders

Iron solution

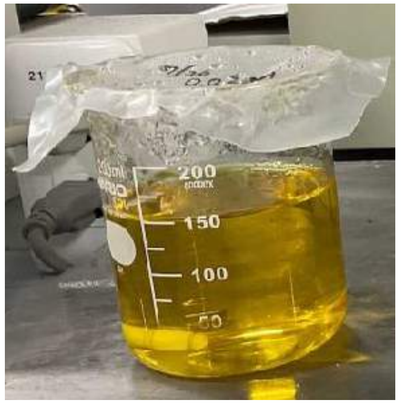

Thin ^{56}Fe absorber

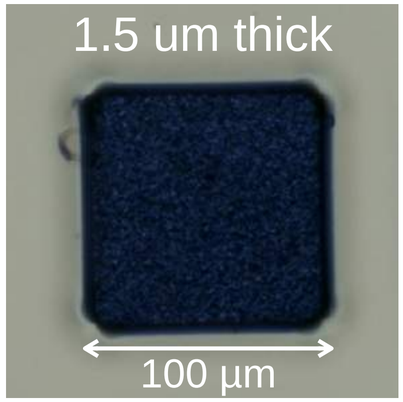

Thermal conductivity of gold

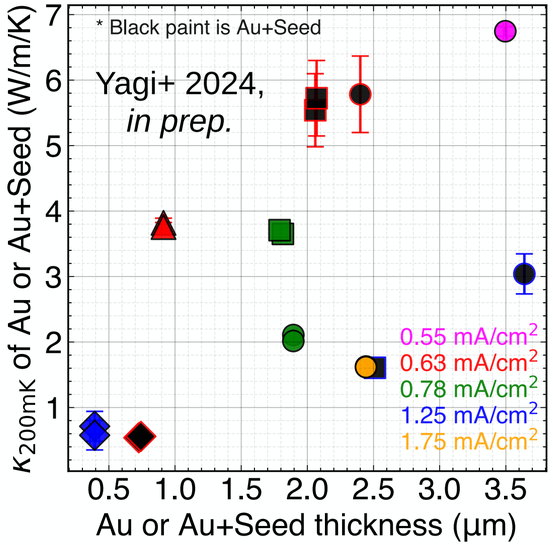

Self-fabricated TES Devices

Test device using ^{56}Fe

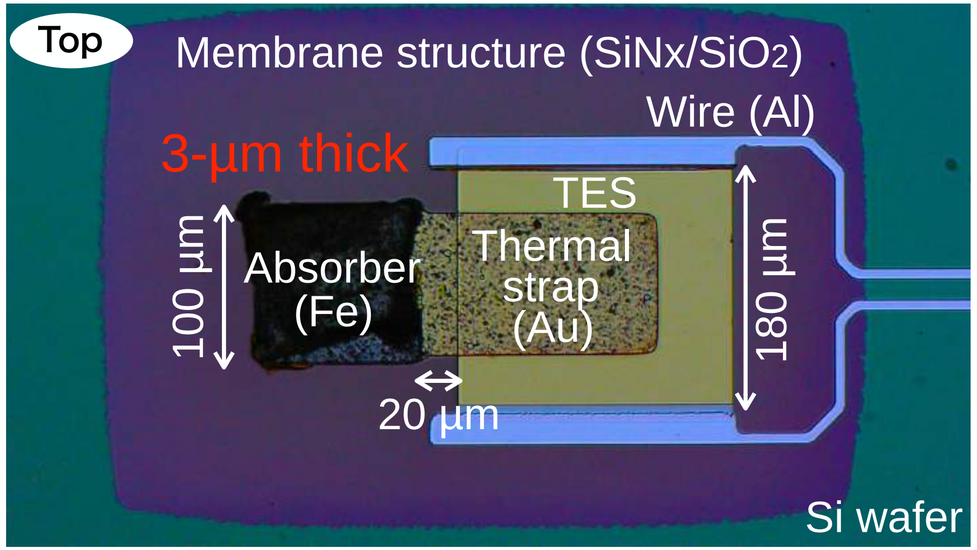

Yagi+ 2023, *J. Low Temp. Phys.*

64-pixel array
+ 12-pixel array

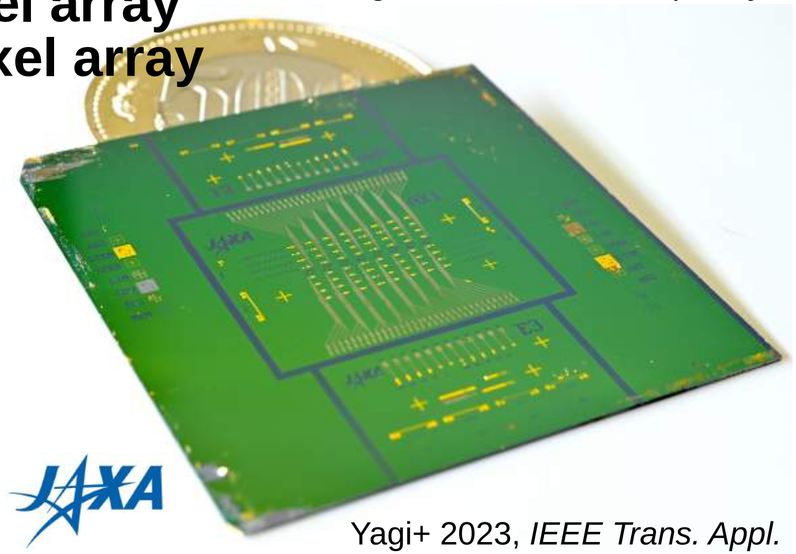

Yagi+ 2023, *IEEE Trans. Appl.*

Test device using ^{57}Fe

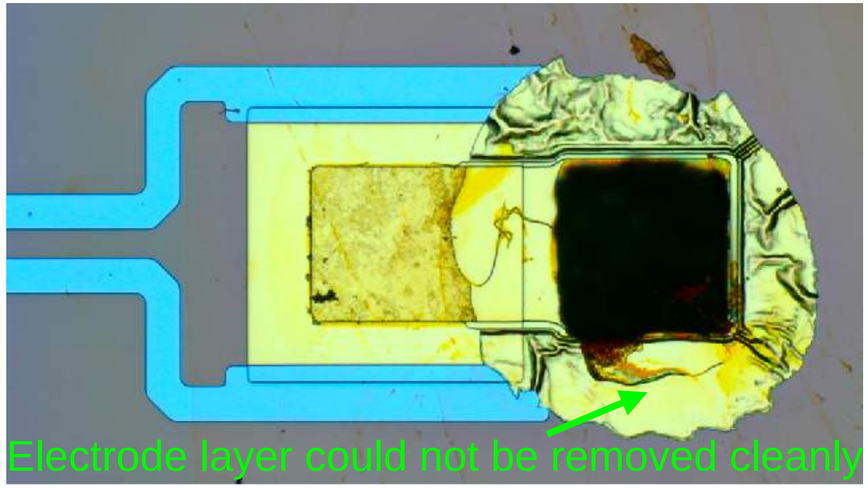

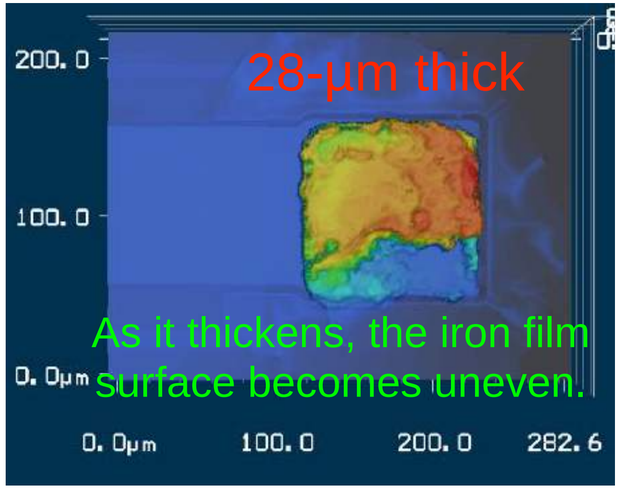

Devices designed with 64 pixels

After Fe deposition process, issues such as peeling and detachment of Fe occur, especially during vacuum cryogenic tests. Currently, less than half of the Fe remains intact.

Use the single-pixel for the first test observation

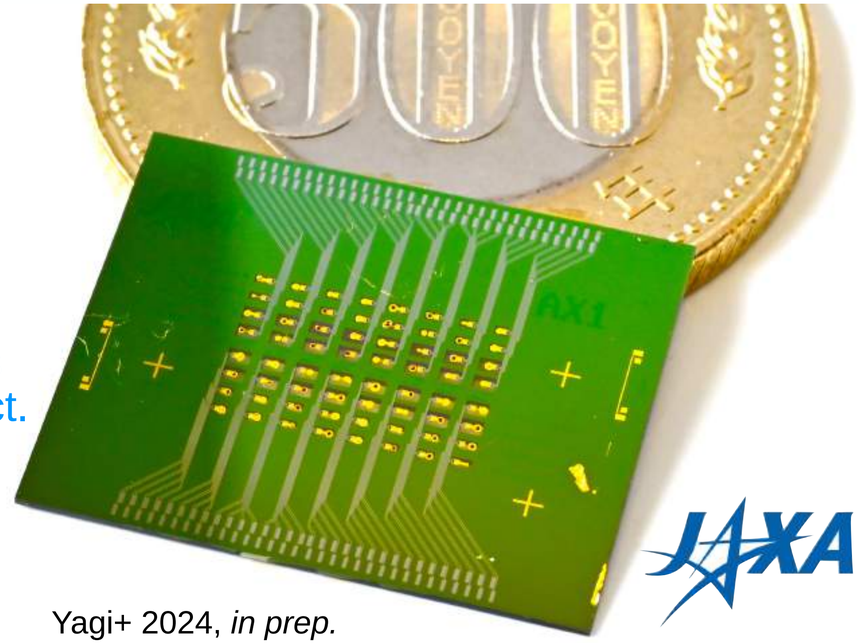

Yagi+ 2024, *in prep.*

Axion observation setup utilizing dilution refrigerator

Dilution refrigerator system

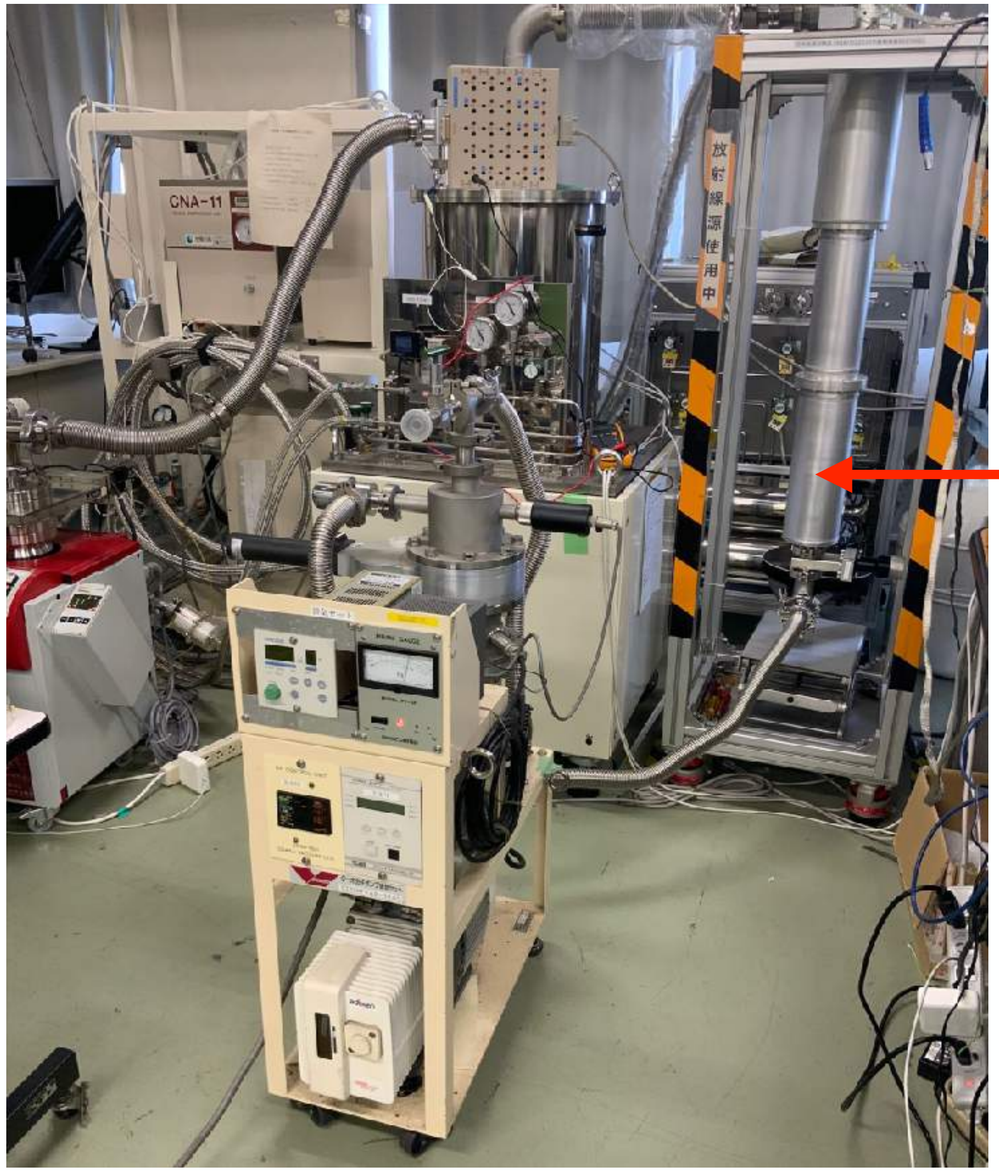

TES stage
(~ 100 mK)

Setup of TES stage with Cu collimator

L-shaped TES stage

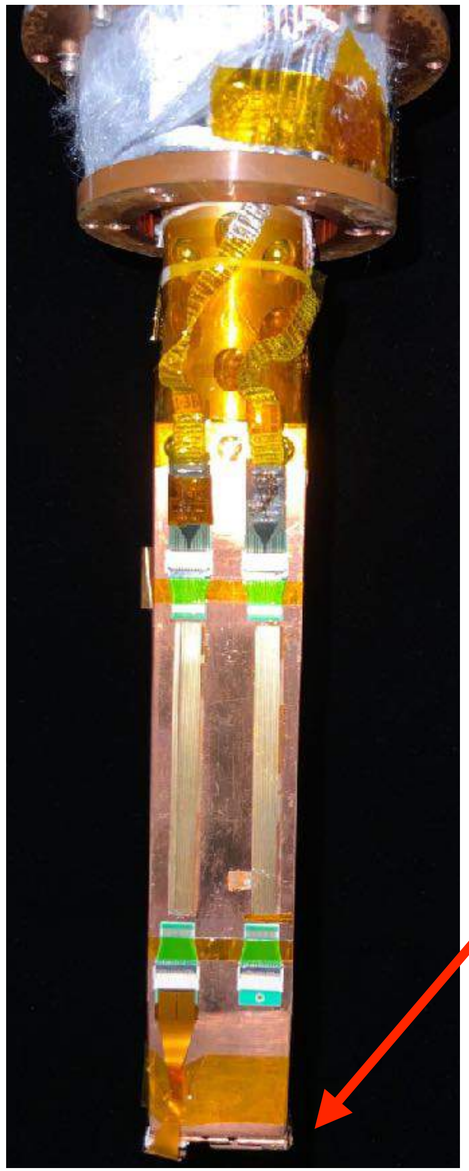

- Conducted tests with single-pixel TES with iron-57 absorber without anti-coincidence detector
- To prevent incoming 14.4 keV radiation other than the absorber, a copper collimator was employed.

Underside of stage

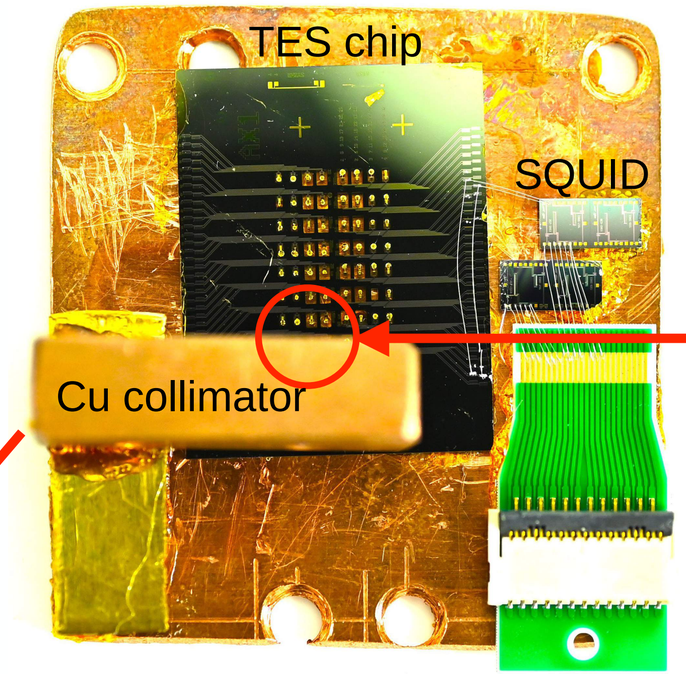

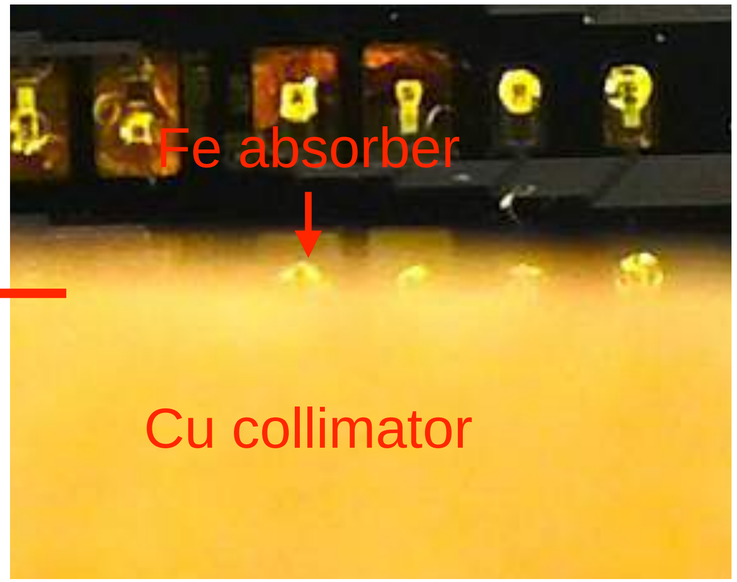

Schematic diagram

Switching mechanism between calibration and observation

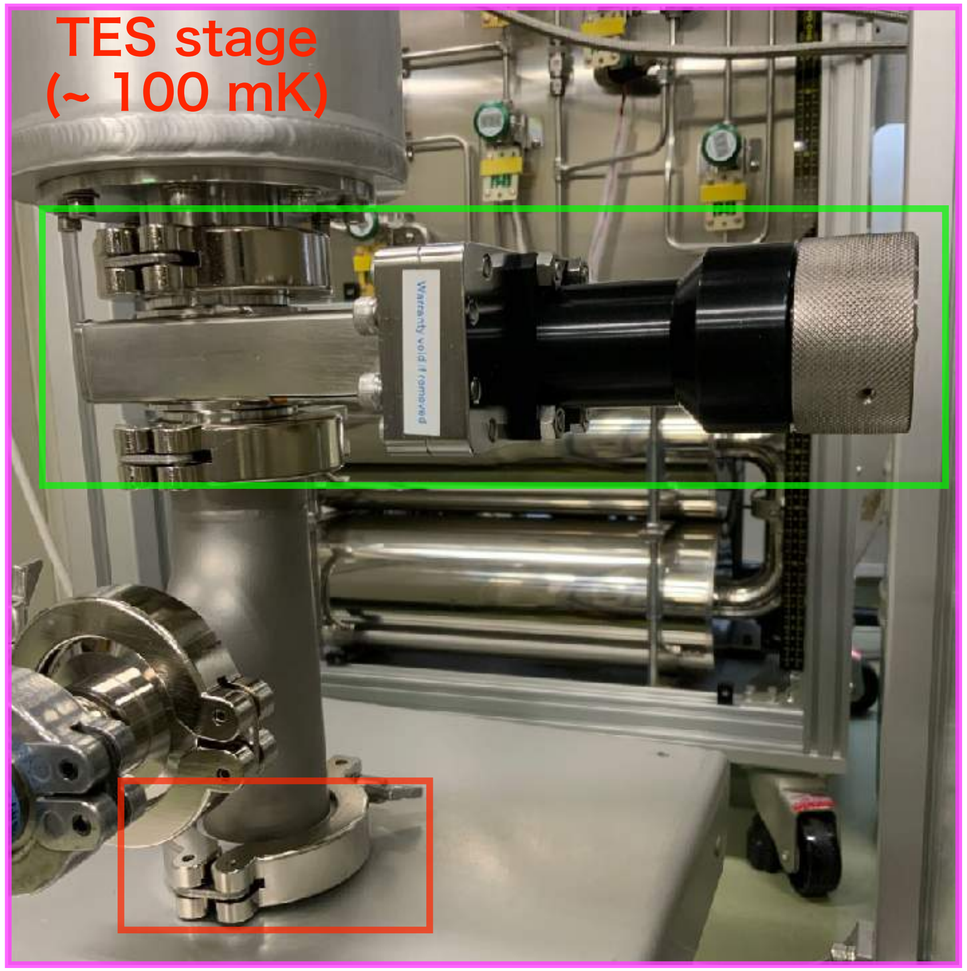

Gate valve (shutter)

OPEN: energy calibration phase

CLOSE: axion search phase

Spectrum of X-rays and gamma rays from ^{57}Co isotope

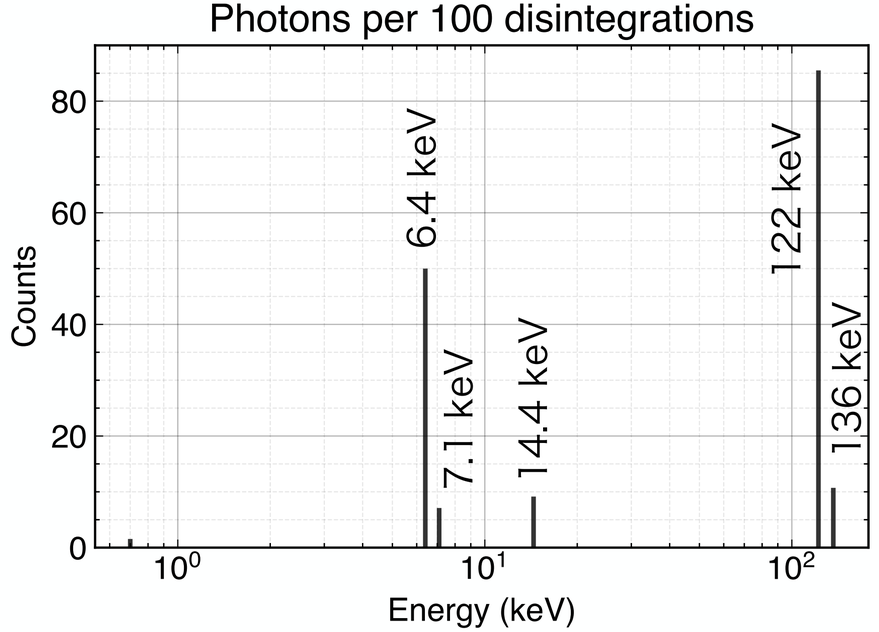

- ^{57}Co decays to ^{57}Fe, emitting 14.4 keV gamma rays, providing an energy calibration source matching axion energy.

Measurement log (Jan. to Feb. 2024)

Gate valve OPEN phase (^{57}Co energy calibration)

Total ~ 10 days

	Chip ID	Observation start	Observation finish	DC or AC	Causes for stopping measurements	Total observation time	Total observation time (sec)
run114	JAXA115 Ax1 2	5:51:00 PM Jan 16 2024	3:41:37 PM Jan 17 2024	AC	PC auto restart	9h 50m 37s	35,437
run116	JAXA115 Ax1 2	4:13:00 PM Jan 28 2024	1:04:55 AM Jan 29 2024	DC	FLL jumping	8h 51m 55s	31,915
run118	JAXA115 Ax1 2	5:21:00 PM Jan 30 2024	9:24:41 AM Jan 31 2024	AC	Manually stopped	16h 3m 41s	57,821
run120	JAXA115 Ax1 2	5:27:00 PM Jan 31 2024	8:56:56 AM Feb 1 2024	AC	Manually stopped	15h 29m 56s	55,796
run122	JAXA115 Ax1 2	5:39:00 PM Feb 1 2024	8:48:04 AM Feb 2 2024	AC	Manually stopped	15h 9m 4s	54,544
run124	JAXA115 Ax1 2	5:54:00 PM Feb 2 2024	9:00:55 AM Feb 3 2024	AC	Manually stopped	15h 6m 55s	54,415
run126	JAXA115 Ax1 2	5:18:00 PM Feb 3 2024	8:59:17 AM Feb 4 2024	AC	Manually stopped	15h 41m 17s	56,477
run128	JAXA115 Ax1 2	5:17:00 PM Feb 4 2024	8:57:54 AM Feb 5 2024	AC	Manually stopped	15h 40m 54s	56,454
run130	JAXA115 Ax1 2	5:23:00 PM Feb 5 2024	8:36:35 AM Feb 6 2024	AC	Manually stopped	15h 13m 35s	54,815
run133	JAXA115 Ax1 2	5:20:00 PM Feb 7 2024	9:57:15 AM Feb 8 2024	AC	Manually stopped	16h 37m 15s	59,835
run135	JAXA115 Ax1 2	7:15:00 PM Feb 8 2024	10:23:10 AM Feb 9 2024	AC	Manually stopped	15h 8m 10s	54,490
run137	JAXA115 Ax1 2	6:04:00 PM Feb 9 2024	3:26:30 PM Feb 11 2024	AC	Manually stopped	45h 22m 30s	163,350
run140	JAXA115 Ax1 2	6:14:04 PM Feb 23 2024	4:32:29 AM Feb 26 2024	DC	Accidental temperature increase	58h 18m 25s	209,905

Gate valve CLOSE phase (Axion search)

Total ~ 4.5 days (Day earth)

	Chip ID	Observation start	Observation finish	DC or AC	Causes for stopping measurements	Total observation time	Total observation time (sec)	Day earth observation time (sec)	Night earth observation time (sec)
run115	JAXA115 Ax1 2	1:00:00 PM Jan 28 2024	4:05:00 PM Jan 28 2024	DC	FLL jumping	3h 5m 0s	11,100	3,122	7,978
run117	JAXA115 Ax1 2	9:50:00 AM Jan 30 2024	1:33:55 PM Jan 30 2024	DC	FLL jumping	3h 43m 55s	13,435	13,435	0
		4:21:00 PM Jan 30 2024	5:14:00 PM Jan 30 2024	DC	Manually stopped	0h 53m 55s	3,180	2,766	414
run119	JAXA115 Ax1 2	-	-	AC	-				
run121	JAXA115 Ax1 2	9:10:00 AM Feb 1 2024	5:32:00 PM Feb 1 2024	AC	Manually stopped	8h 22m 0s	30,120	28,751	1,369
run123	JAXA115 Ax1 2	8:55:00 AM Feb 2 2024	5:47:00 PM Feb 2 2024	AC	Manually stopped	8h 52m 0s	31,920	29,713	2,207
run125	JAXA115 Ax1 2	9:04:00 AM Feb 3 2024	5:13:00 PM Feb 3 2024	AC	Manually stopped	8h 9m 0s	29,340	29,235	105
run127	JAXA115 Ax1 2	9:03:00 AM Feb 4 2024	5:13:00 PM Feb 4 2024	AC	Manually stopped	8h 10m 0s	29,400	29,357	43
run129	JAXA115 Ax1 2	9:01:00 AM Feb 5 2024	5:19:00 PM Feb 5 2024	AC	Manually stopped	8h 9m 0s	29,880	29,539	341
run131	JAXA115 Ax1 2	8:40:00 AM Feb 6 2024	5:17:00 PM Feb 6 2024	AC	Manually stopped	8h 37m 0s	31,020	30,861	159
run132	JAXA115 Ax1 2	10:50:00 AM Feb 7 2024	5:16:00 PM Feb 7 2024	AC	Manually stopped	6h 26m 0s	23,160	23,123	37
run134	JAXA115 Ax1 2	10:00:00 AM Feb 8 2024	5:18:00 PM Feb 8 2024	AC	Manually stopped	7h 18m 0s	26,280	26,184	96
run136	JAXA115 Ax1 2	10:26:00 AM Feb 9 2024	6:00:00 PM Feb 9 2024	AC	Manually stopped	7h 34m 0s	27,240	24,685	2,555
run138	JAXA115 Ax1 2	3:33:00 PM Feb 11 2024	2:15:15 PM Feb 14 2024	AC	Manually stopped	70h 42m 15s	254,535	112,075	142,460
run139	JAXA115 Ax1 2	11:07:00 AM Feb 16 2024	5:32:00 PM Feb 16 2024	AC	Manually stopped	6h 25m 0s	23,100	22,647	453

58 hours energy calibration with single-pixel TES

- Reporting select data with a more advanced understanding of events.
- Conducted about 58 hours of energy calibration measurement (run140)

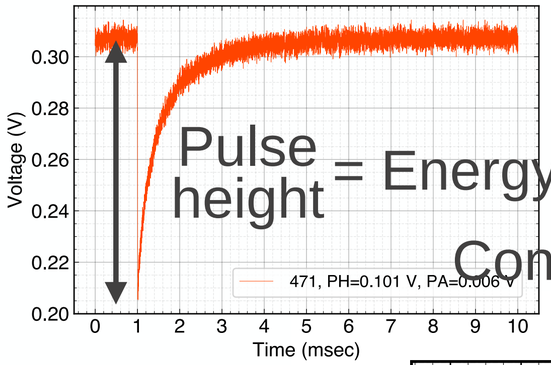

Energy calibration measurement (~ 58 h)

Converting pulse height to energy

Energy spectrum

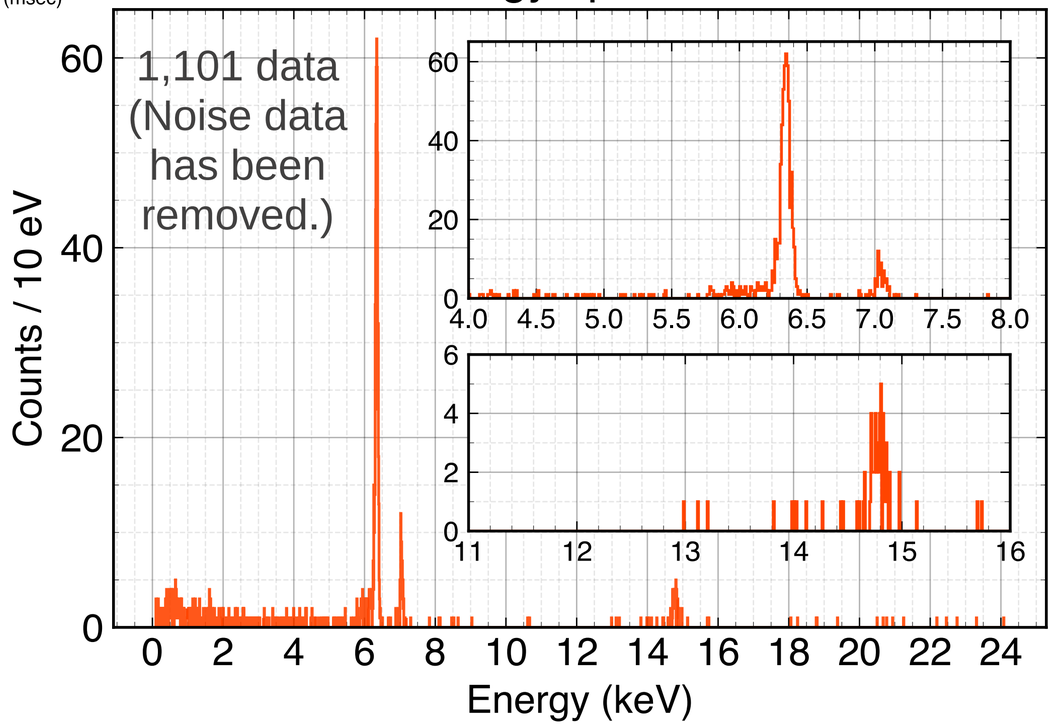

Gaussian fit of major peaks data

Energy resolution by Gaussian

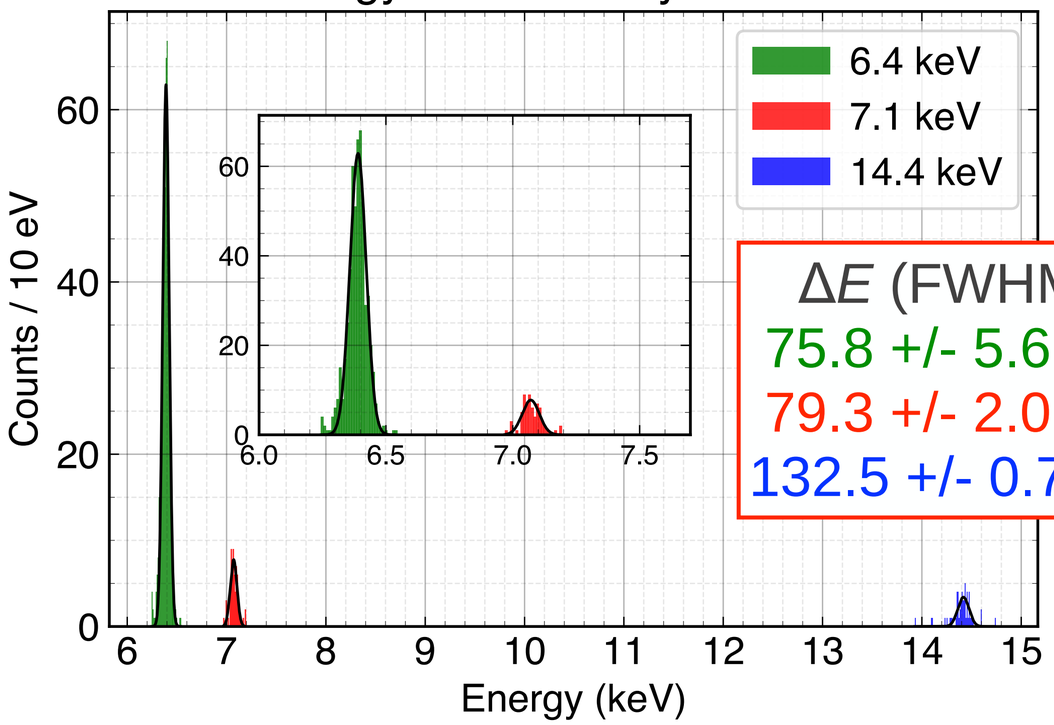

ΔE (FWHM)
75.8 +/- 5.6 eV
79.3 +/- 2.0 eV
132.5 +/- 0.7 eV

Unexpected event

Conventionally follows a linear relationship

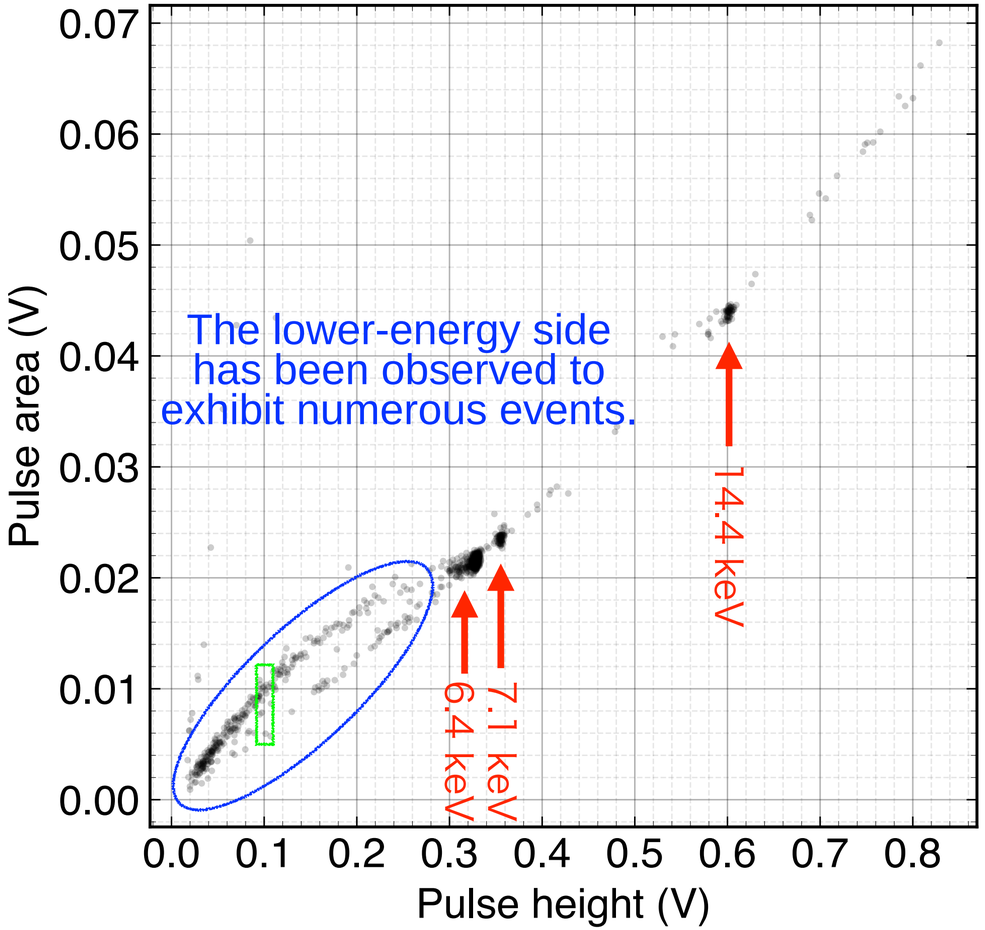

$$\text{Pulse height (V)} = \text{Baseline} - \text{Peak}$$

$$\text{Pulse area (V)} = \frac{\int_{0\text{ms}}^{10\text{ms}} (\text{Baseline} - V(t))dt}{\int_{0\text{ms}}^{10\text{ms}} dt}$$

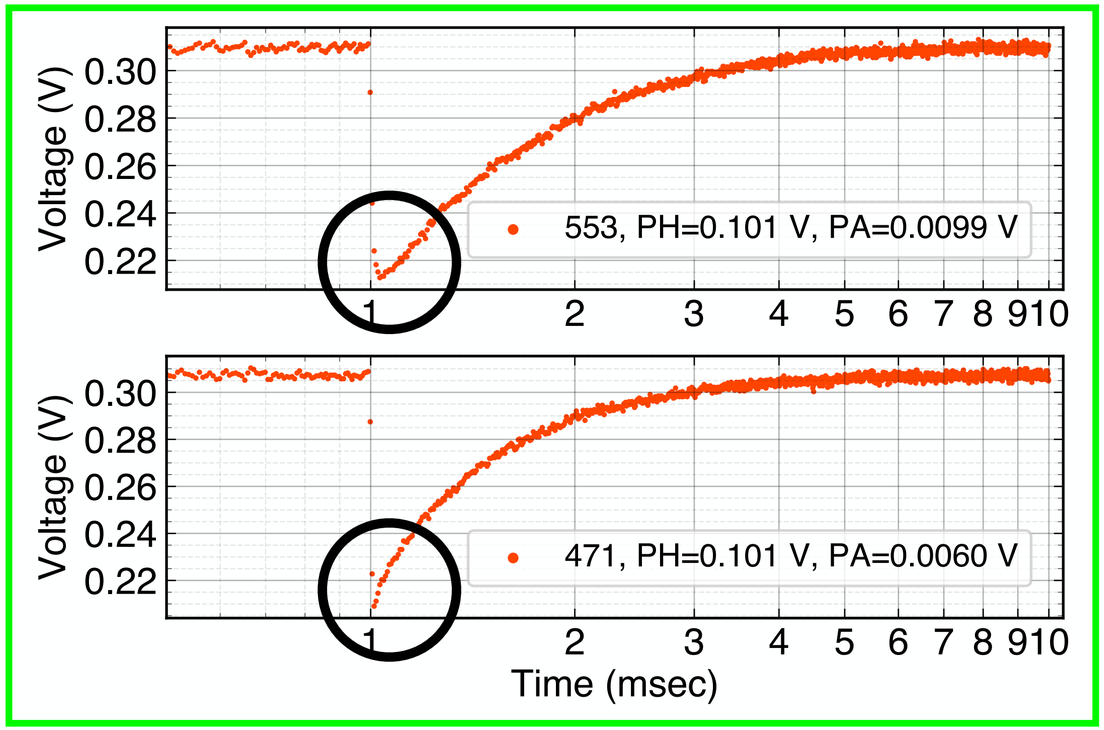

- Waveforms were observed where the pulse height remained the same, but the pulse area slightly differed.
- The slight waveform differences may potentially indicate distinctions between absorber events and strap events.
- It is essential to understand the events thoroughly and impose constraints on the axion observation data accordingly.

We're still in the process of understanding the events.

4.5 hours solar axion search with single-pixel TES

- Reporting select data with a more advanced understanding of events.
- Conducted about 4.5 hours of axion observation (run117)
- Seven events were measured.

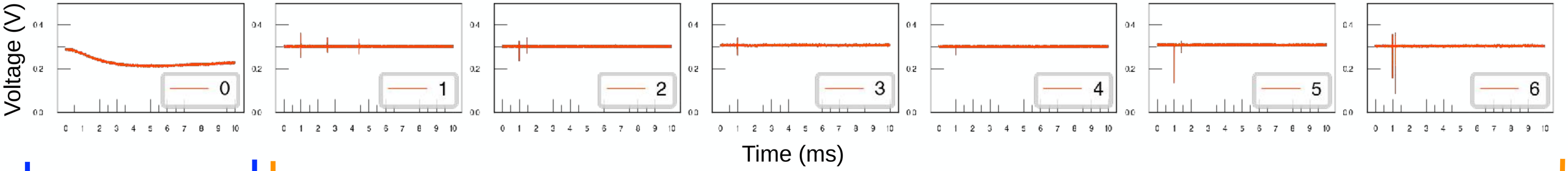

Events No. 0 is associated with the TES substrate event.

Events No. 1 to No. 6 are attributed to electrical shot noise.

Given the short observation time for the data used here,
background events such as cosmic ray events were not observed.

→ With improved waveform understanding in calibration phase, additional data can be incorporated, allowing for background rate calculations and axion mass constraints.

Future constraint on the axion mass

Using the obtained excitation rate from observations to place constraints on the axion mass.

$$R = 3.1 \times 10^2/\mathrm{day/kg} \left(\frac{10^6\ \mathrm{GeV}}{f_a} \right)^4 C^4$$ Moriyama 1995, revised

$$m_a = \frac{\sqrt{z}}{1+z} \frac{f_\pi m_\pi}{f_a} = 1\ \mathrm{eV} \frac{\sqrt{z}}{1+z} \frac{1.3 \times 10^7}{f_a/\mathrm{GeV}} \quad (m_\pi = 139\ \mathrm{MeV}, f_\pi = 93\ \mathrm{MeV})$$

The plan is to impose a mass limit of a few keV or less based on short observations (a few hours) with single-pixel TES.

e.g. Namba 2007, *Phys. lett. B*

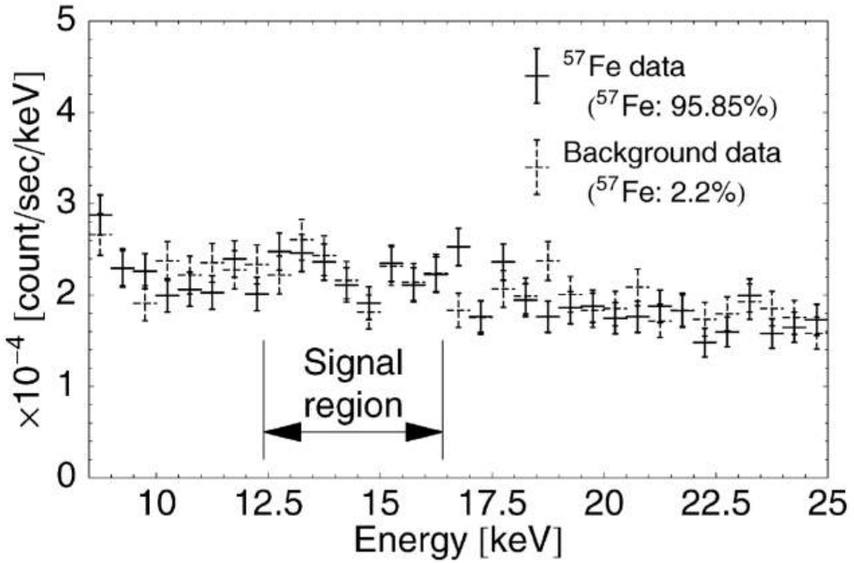

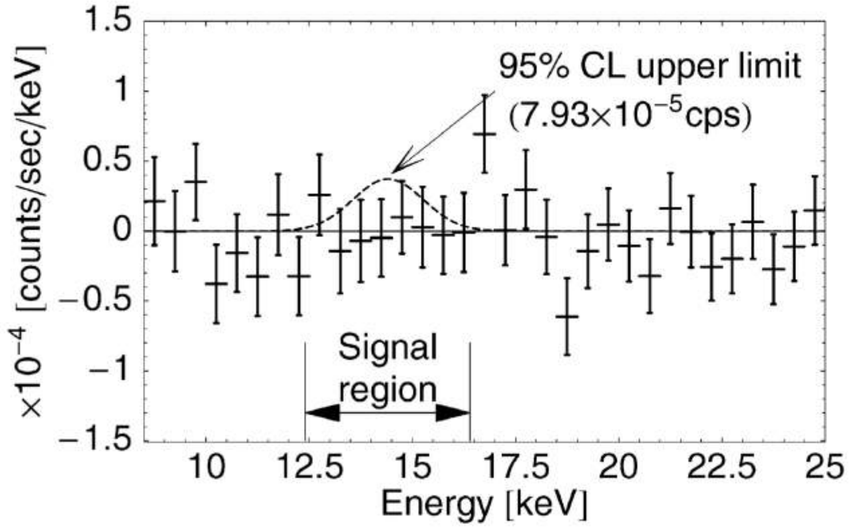

$$R < \frac{N_\gamma}{M_{57} \cdot \gamma_E \cdot \epsilon} = \frac{7.12\ \mathrm{day}^{-1}}{197\ \mathrm{mg} \cdot 0.105 \cdot 0.148}$$
$$= 2.33 \times 10^6\ \mathrm{day}^{-1}\,\mathrm{kg}^{-1}.$$

$m_a < 216$ eV (95 % C.L.)

Summary

★ TES microcalorimeter is promising for the most stringent bound for observations with 57Fe.

★ Conducted the first solar axion observation using a TES with a 57Fe absorber.

★ Unexpected events were observed, and investigations are currently underway to understand them.

★ Once event classification is established, preliminary constraints on the axion mass can be applied, paving the way for future high-sensitivity observations with an array.